Effectively and Efficiently Dissecting the Infection of Influenza Virus by Quantum-Dot-Based Single-Particle Tracking

Shu-Lin Liu,[†] Zhi-Ling Zhang,[†] Zhi-Quan Tian,[†] Hai-Su Zhao,[†] Haibin Liu,[‡] En-Ze Sun,[†] Geng Fu Xiao,[‡] Wanpo Zhang,[‡] Han-Zhong Wang,[‡] and Dai-Wen Pang[†,*]

[†]Key Laboratory of Analytical Chemistry for Biology and Medicine (Ministry of Education), College of Chemistry and Molecular Sciences, Research Center for Nanobiology and Nanomedicine (MOE 985 Innovative Platform), State Key Laboratory of Virology, and Wuhan Institute of Biotechnology, Wuhan University, Wuhan 430072, People's Republic of China, and [‡]State Key Laboratory of Virology, Wuhan Institute of Virology, Chinese Academy of Sciences, Wuhan 430071, People's Republic of China

ABSTRACT Exploring the virus infection mechanisms is significant for defending against virus infection and providing a basis for studying endocytosis mechanisms. Single-particle tracking technique is a powerful tool to monitor virus infection in real time for obtaining dynamic information. In this study, we reported a quantum-dot-based single-particle tracking technique to efficiently and globally research the virus infection behaviors in individual cells. It was observed that many influenza viruses were moving rapidly, converging to the microtubule organizing center (MTOC), interacting with acidic endosomes, and finally entering the target endosomes for genome release, which provides a vivid portrayal of the five-stage virus infection process. This report settles a long-pending question of how viruses move and interact with acidic endosomes before genome release in the perinuclear region and also finds that influenza virus infection is likely to be a "MTOC rescue" model for genome release. The systemic technique developed in this report is expected to be widely used for studying the mechanisms of virus infection and uncovering the secrets of endocytosis.

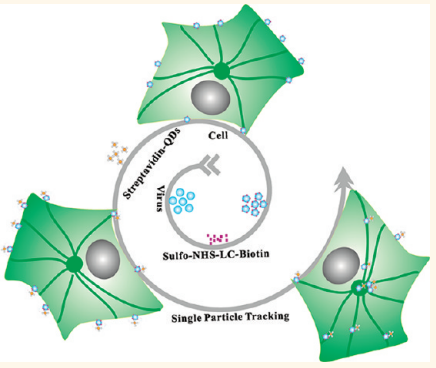

KEYWORDS: influenza virus · quantum dot · infection · single-particle tracking · endocytosis · bionanotechnology

As obligate parasites, many viruses utilize endocytosis to infect host cells for replication.[1−5] It is momentous to explore the infection mechanisms for fighting with virus infection and obtaining valuable information on endocytosis. Virus infections are complex processes, which involve many steps and interactions between viruses and various cellular structures.[5−7] Due to these dynamic interactions and diverse routes of viruses infecting cells, single-virus tracking technique is badly needed to monitor the virus infection behaviors in real time and long term to further dissect the infection mechanisms within the cell and to understand the processes of endocytosis.[5,8−10]

Influenza A virus is an enveloped virus that belongs to the Orthomyxoviridae family, a group of single-stranded minus-sense RNA viruses with a segmented genome.[11,12] Natural infections of influenza A viruses have been reported in humans and a variety of animal species, including horses, swine, and birds.[13−15] Avian influenza A viruses are renowned for causing the largest, most devastating outbreak of infectious diseases in modern history[13−17] and are considered as potential risks to public health.[11,12,14,16] Owing to the frequent occurrence of antigenic drift and shift, presently, there is no very effective way to prevent or treat influenza infection.[11,13,14] Thus, a better understanding of the influenza infection pathway is required to develop novel strategies for preventing and lessening the influence of the next pandemic. Influenza virus processes a multistep infection process in live cells: viruses enter into cell *via* receptor-mediated endocytosis, move along actin filaments and microtubules, and fuse with late endosomes.[3,6,18−20] However, many critical issues regarding the infection of influenza virus remain obscure. For example, the scenario of the infection behaviors (especially in the perinuclear region) and the interactions between viruses and cell organelles before genome release remain rarely understood. Moreover, the population infection behaviors in individual cells remain poorly monitored in real time and long term.

* Address correspondence to dwpang@whu.edu.cn.

Received for review August 16, 2011 and accepted November 25, 2011.

Published online November 25, 2011
10.1021/nn2031353

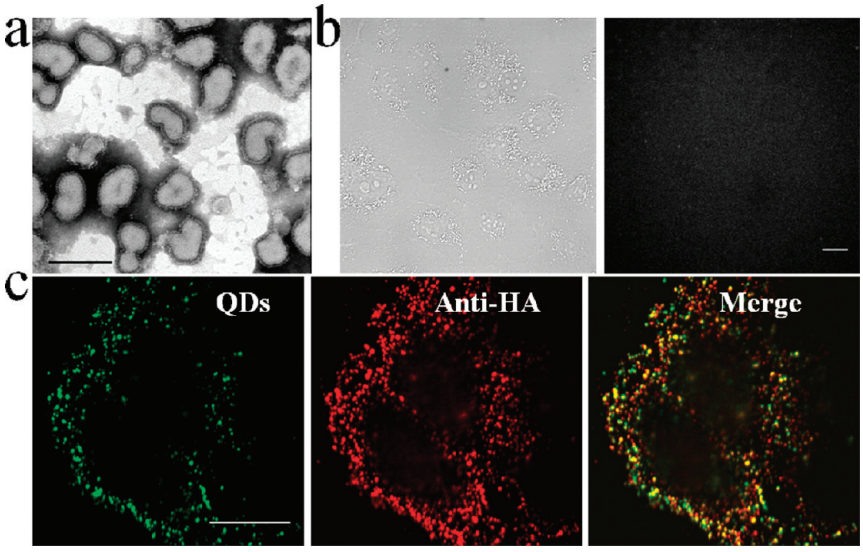

Figure 1. Specificity and sufficiency of quantum dots (QDs) as tags to label viruses. (a) Electron micrograph of purified H9N2 viruses (scale bar, 200 nm). (b) Differential interference contrast (DIC) image and fluorescence image of the cells incubated with streptavidin-modified QDs (SA-QDs) alone (scale bar, 20 μm). (c) Fluorescence image of QD-labeled viruses (green), immunofluorescence image of hemagglutinin (HA) (red), and the merge of immunofluorescence image with the QD image in a cell. Pixels with both red and green signals appear yellow (scale bar, 20 μm).

Semiconductor quantum dots (QDs) have unique optical properties such as superior photostability and high brightness, which have fascinated researchers in the biomedical field over the past decade.[21−27] Especially, QDs have been used in the field of single-particle tracking.[28−30] In an effort to study the virus infection mechanism, we utilized QDs as tags to investigate the transport behaviors of prion and infectious hematopoietic necrosis virus.[31,32] Wang *et al.* used QDs to label adeno-associated virus for studying the intracellular behaviors in living target cells.[33] However, a QD-based systemic technique for effectively and efficiently studying the global infection behaviors of viruses in individual cells has not been provided so far.

In this work, we developed a QD-based single-particle tracking technique to dissect the infection behaviors of H9N2 influenza viruses in individual cells. This allowed us to globally characterize the infection process by effectively and efficiently analyzing the behaviors of viruses in individual cells. Long-term tracking of multiple viruses in one cell indicated that the movements of viruses exhibited a directed, parallel, and regular motional pattern in the cytoplasm. Individual trajectories' analysis revealed that the virus infection was a typical five-stage process. Simultaneous tracking of viruses and acidic endosomes showed that the viruses moved intermittently around the microtubule organizing center (MTOC) by interacting with acidic endosomes and finally entered acidic endosomes. The QD-based single-particle tracking makes it convenient to systemically studying the infection process, which would help us to obtain previously unavailable information about the dynamics of the population infection behaviors and the interaction between viruses and cell organelles.

RESULTS AND DISCUSSION

Specificity and Sufficiency of QDs as Tags To Label Viruses. In this study, H9N2 viruses were propagated in embryonated eggs and purified by ultracentrifugation (see Materials and Methods). The TEM image showed that the virions were intact (Figure 1a). The purified H9N2 viruses were labeled with QDs to visualize individual influenza particles in Madin−Darby canine kidney (MDCK) cells. The QD-labeled viruses distributed discrete fluorescent structures on the cell surface (Figure 1c left). In the negative control experiment (adding streptavidin-modified QDs (SA-QDs) alone) (Figure 1b), few fluorescence signals were detected on the cell surface, indicating that SA-QDs could bind specifically to the viruses on the cell surfaces. To test whether the QD signals exhibit viruses adequately, we immunolabeled virus particles with an antibody against hemagglutinin (HA), a glycoprotein on the surface of influenza virus (Figure 1c middle).[34] Over 95% of discrete structures in the QDs image colocalized with those in the immunofluorescence image (Figure 1c right), illustrating that the QD signals were specific and adequate to exhibit the virus particles in live cells. Additionally, the influence of the labeling on virus infectivity was examined by 50% tissue culture infectious dose (TCID 50) and immunofluorescence focus assay, respectively (Figure S1 in Supporting Information). The virus infectivity decreased slightly after labeling with QDs, suggesting that the labeled viruses were still infectious and the labeling had less influence on the virus infectivity. These results suggested that the labeling strategy was feasible to label the viruses with QDs.

Simultaneous and Long-Term Tracking Multiple Virus Behaviors in Individual Cells. To investigate the population

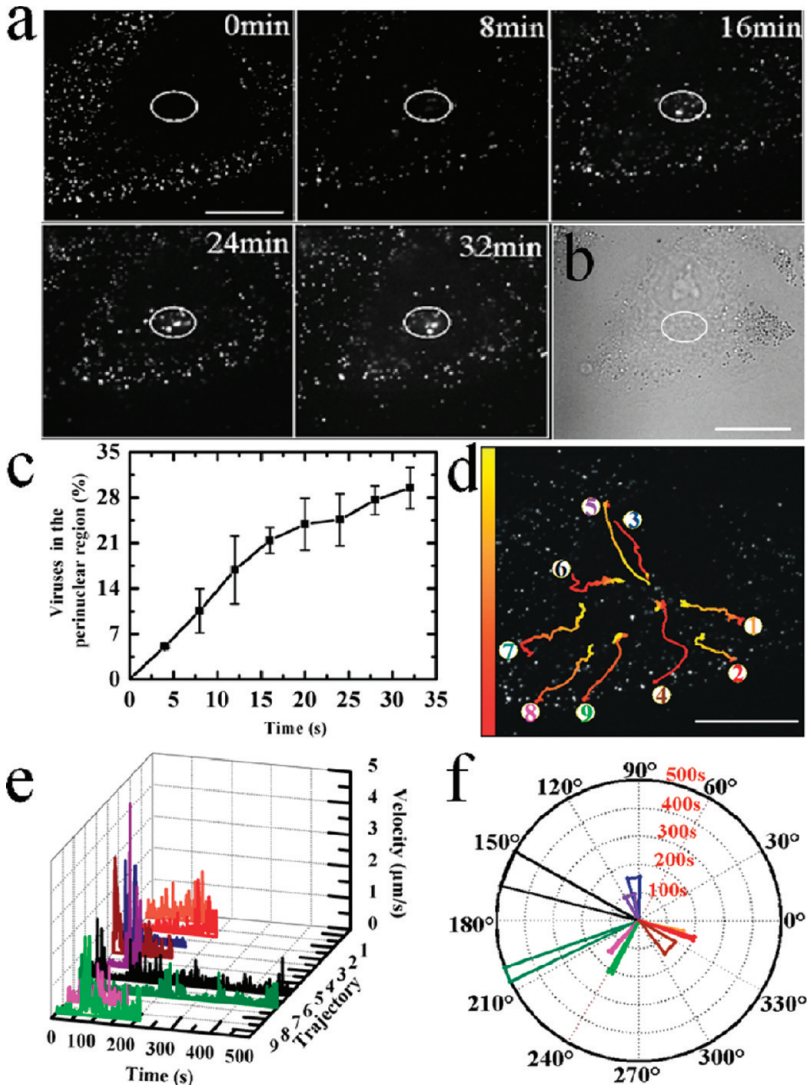

Figure 2. Tracking the individual viruses in a cell. (a) Snapshots of the viruses traveling in a live cell. The white circle indicates the converging region in the cell. (b) DIC image of the cell. (c) Percentage of viruses in the perinuclear region over time. (d) Nine trajectories of the virus transports in the cell. The color of the trajectories with the colored bar indicates a time axis from red to yellow (scale bar, 20 μm), and the trajectories are labeled with different colored numbers. (e) Instantaneous speed−time plots of the nine viruses. (f) Polar plots of the nine viruses. The nine angle bins indicate the nine trajectories. The colors are consistent with the colored numbers of the different trajectories shown in (d). The direction of each bin indicates the virus moving direction. The angle range of each bin indicates the angle range of the virus traveling relative to the perinuclear region. The radius indicates the traveling time of the virus.

behaviors of viruses, we infected MDCK cells with about 100 μg/mL viruses, which allowed us to discern individual virus particles and met the need for monitoring the population behaviors of viruses in live cells. Many viruses in individual cells were simultaneously tracked and imaged with a frame interval of 500 ms for about 30 min (Figure 2a). It was found that the viruses were maintained on the cell surface at 0 min postinfection. Over time, viruses appeared in the cytoplasm and accumulated at a special region inside the cell (highlighted by a white circle). The differential interference contrast (DIC) image of the cell (Figure 2b) suggested that the viruses accumulated in a perinuclear region. Counting the viruses in this region (Figure 2c), nearly 25% of the viruses had been transported to this region within 20 min postinfection. However, only about 30% of the viruses accumulated to this region within 30 min postinfection, suggesting that the accumulation had been slow to rise after 20 min postinfection. The virus population movements within 8 min postinfection (see movie S1 in Supporting Information) were analyzed to investigate the dynamics of infection behaviors. Interestingly, many viruses initially stayed on the cell surface, moved slowly around the cytomembrane, subsequently traveled rapidly with a directed, parallel, and regular motional pattern in the cytoplasm, and finally converged to the perinuclear region. One thing deserves our attention is that nearly all of the internalized viruses were associated with a unidirected rapid movement toward the perinuclear region, indicating

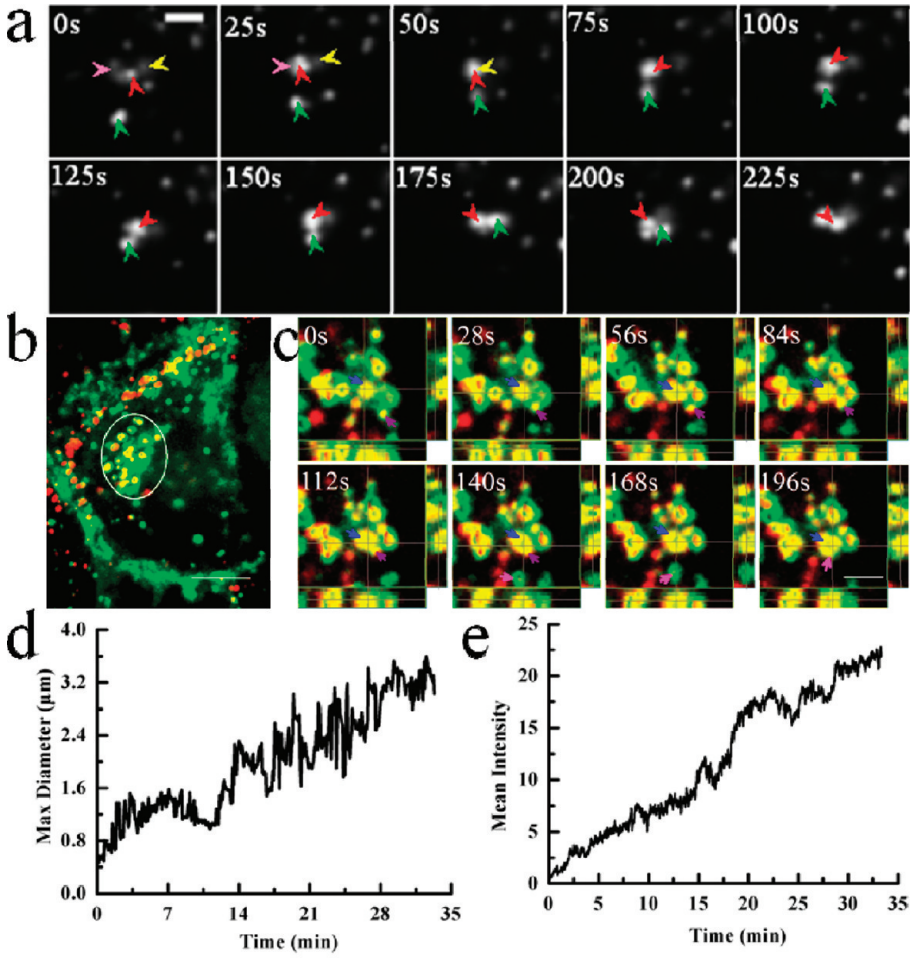

Figure 3. Tracking the aggregating process of the vesicles containing viruses. (a) Snapshots of the fusion process between the vesicles (scale bar, 2 μm). (b) Colocalization (yellow) of the QD-labeled viruses (red) with DiO-labeled vesicles (green) in the cytoplasm (scale bar, 10 μm). The white circle indicates the virus accumulation region in the cytoplasm. (c) Orthogonal slice images of the vesicle-to-vesicle fusing process in the perinuclear region. Each time point is shown as the merge image of QD−H9N2 (red) and the cell membrane stained with DiO (green) (scale bar, 5 μm; gap of $Z = 0.5$ μm). Clearly, the last image shows that the three vesicles had fused whenever observed from $x-y$, $x-z$, and $y-z$ plane. (d) Max diameter−time plot in the perinuclear region. (e) Mean intensity−time plot in the perinuclear region.

that the movement near the cytomembrane may be the "rate-determining" step for virus entry. The individual trajectories of viruses (Figure 2d) demonstrated that the viruses were converging to the perinuclear region from all directions. The time trajectories of the virus instantaneous speed (the distances between two adjacent frames divided by the frame interval time) showed that most viruses exhibited a slow-fast-slow pattern to the perinuclear region (Figure 2e), indicating that the movement may be related to different components successively, such as actin filaments and microtubules.[3] With the center of the perinuclear region as a pole, the polar plots of the trajectories distinctly suggested that viruses were traveling in the cytoplasm with the angle range of 1−10°. The results indicated that the virus infection was a very regular process in the complex, heterogeneous interior of the cell (Figure 2f).

The perinuclear region (the white circle in Figure 2a) was focused to further investigate virus movements in detail. As shown in Figure 3a, it was very interesting to discover that several light spots accumulated together (see movie S2 in Supporting Information). One of the light spots (red arrow) was maintained at one position, which merged with the other three spots at 25 s (pink arrow), 50 s (yellow arrow), and 200 s (green arrow). The instantaneous speed of the spots moving toward the designated one was about 0.4 μm/s. Tracking the QD-labeled viruses in MDCK cells stained with DiO (a membrane dye), we found that the QD-labeled viruses were colocalized with DiO in the cytoplasm (especially in the perinuclear region, highlighted with white circle) (Figure 3b), indicating that the viruses in vesicles were transported in the cytoplasm. Further investigating the movement in the perinuclear region, vesicle−vesicle fusion was observed (Figure 3c and movie S3 in Supporting Information). Thus, it could be concluded that the light spots' accumulation was a vesicle−vesicle fusion event. Additionally, the maximal diameter of the vesicle in this region increased gradually, suggesting that the vesicles containing viruses were growing

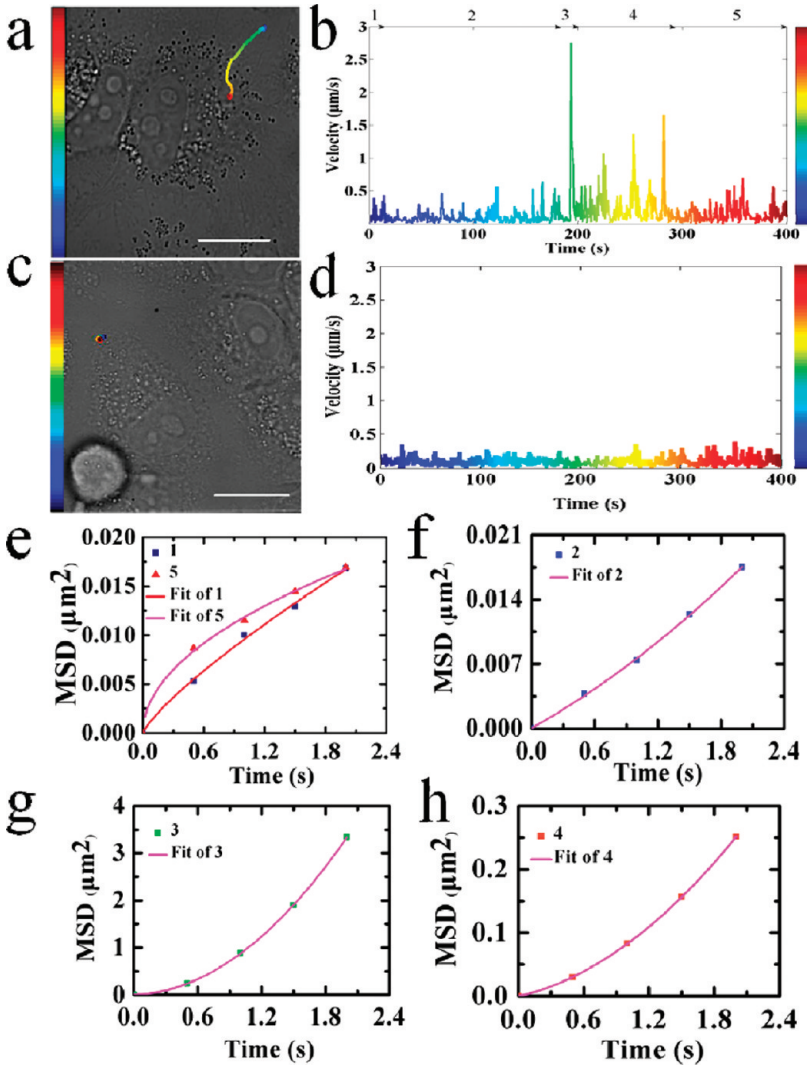

Figure 4. Analyzing the transport of individual influenza viruses in live cells. (a) Trajectory of a virus inside a cell. (b) Time trajectory of the instantaneous speed of the virus shown in (a). (c) Typical trajectory of a virus inside a nocodazole-treated cell. (d) Time trajectory of the instantaneous speed of the virus shown in (c). Numbers 1, 2, 3, 4, and 5 are the durations of stage 1, stage 2, stage 3, stage 4, and stage 5, respectively (scale bar, 20 μm). The color of the trajectory with the colored bar indicates a time axis from 0 s (blue) to 400 s (red). (e) Mean square displacement (MSD)−time plots in stage 1 (dark blue symbols) and stage 5 (plum symbols). The red and purple lines are the fits to MSD = $4D\tau^{\alpha}$ + constant (the constant term was due to noise and $\alpha < 1$) in stage 1 and stage 5, respectively. (f−h) MSD−time plots in stage 2 (blue symbols), stage 3 (green symbols), and stage 4 (red symbols). The purple lines are the fits to MSD = $4D\tau + (V\tau)^2$ + constant (the constant term was due to noise).

up within 30 min postinfection (Figure 3d). Meanwhile, the mean fluorescence intensity of this region increased over time, indicating that the viruses were indeed converging to this region (Figure 3e). The results suggested that many viruses may finally be transported into the same organelle. The relation between the vesicle−vesicle fusion and the virus−endosome fusion remained to be investigated.

Five-Stage Transport Pattern of Virus Infection. To reveal the infection pathway unambiguously, we analyzed the individual virus trajectories in live cells in detail. The typical trajectory of the virus moving in MDCK cell is shown in Figure 4a and movie S4 in Supporting Information. Herein, on the basis of the position and the instantaneous speed in the cell, the infection process was dissected into a previously unreported five-stage transport pattern: the viruses being restricted initially on the cell surface (stage 1), moving slowly in the cell periphery (stage 2), traveling rapidly toward the cell nucleus (stage 3), moving intermittently in the perinuclear region (stage 4), and finally moving confinedly in this region (stage 5) (Figure 4b).

Subsequently, we investigated the mechanisms of the virus movement in each stage. According to the dependence of mean square displacement (MSD) on time (τ), the movements could be characterized as free diffusion (linear relation, MSD = $4D\tau$), directed motion along cytoskeletons (upward curvature, MSD = $4D\tau + (V\tau)^2$), and anomalous diffusion within a confined region (downward curvature, MSD = $4D\tau^{\alpha}$) (D and V are the diffusion coefficient and velocity of the particle, respectively; α is a coefficient and $\alpha < 1$).[35,36] Stage 1

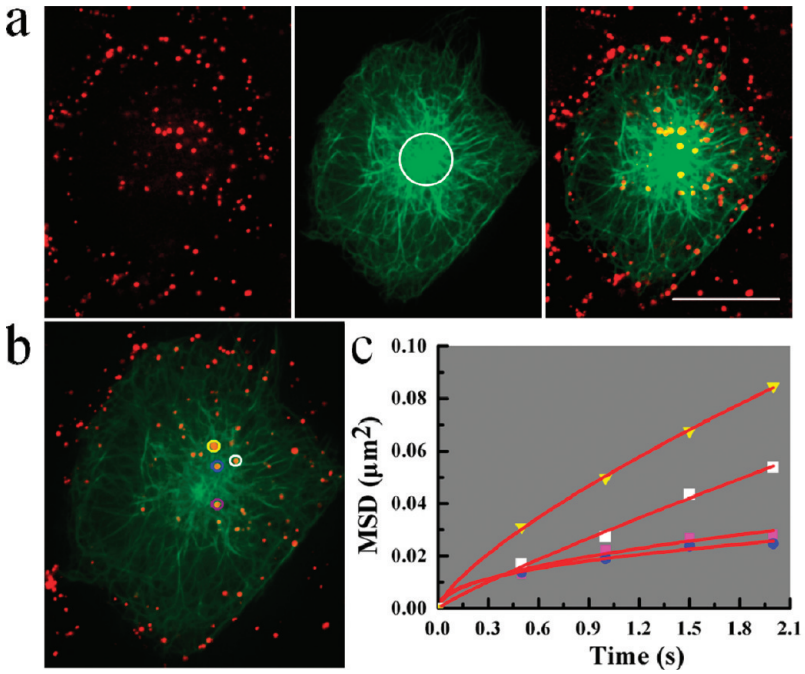

Figure 5. Converging site of the viruses in live cells. (a) Fluorescence images of MDCK cells expressing green fluorescence protein (GFP)-tagged microtubules (green), QD-labeled viruses (red), and the merge (scale bar, 20 μm). The white circle indicates the microtubule organizing center (MTOC). (b) Example of the vesicles moving around the MTOC. Four vesicles are indicated with different colors. (c) MSD−time plots of the four vesicles' movements. The different color symbols indicate the different vesicles shown in (b). The red lines are the fits to MSD = $4D\tau^{\alpha}$ + constant.

represented the movement after the initial binding of viruses to the cytomembrane. The dependence of MSD on time showed that the stage 1 movement was in anomalous diffusion mode with D and α values of 0.002 μm^2/s and 0.8, respectively, which could be speculated that the viruses were blocked by the cytomembrane initially and trapped into vesicles (Figure 4e).[18]

Stage 2 indicated the long-time and slow movement in the cell periphery after stage 1. The dependence of MSD on time in this stage showed that the movement was slow and directed with D and V values of 0.002 μm^2/s and 0.03 μm/s, respectively (Figure 4f). To ascertain the mechanisms associated with the transport, we tracked the viruses in MDCK cells transiently expressing green fluorescent protein (GFP)-tagged actin filaments. The virus was moving slowly on actin filaments in the cell periphery (Figure S2a in Supporting Information). The whole trajectory and the upward-curving MSD−time plot of the virus movement (Figure S2b,c in Supporting Information) showed that the movements on actin filaments were indeed slow and directed with D and V values of 0.003 μm^2/s and 0.04 μm/s, respectively, consistent with the values in the previous report.[3] The results suggested that the stage 2 movement was actin-dependent.

Stage 3 was the fast and unidirected movement from the cell periphery to the perinuclear region after stage 2. The dependence of MSD on time in this stage showed that the virus movement in stage 3 was directed with D and V values of 0.021 μm^2/s and 0.89 μm/s, respectively (Figure 4g). Tracking the viruses in MDCK cells transiently expressing GFP-tagged microtubules, we found that the virus was moving rapidly on microtubules from the cell periphery to the nucleus (Figure S3 in Supporting Information). The whole trajectory and the upward-curving MSD−time plot of the trajectory showed that the movement of the particle was fast and directed with D and V values of 0.035 μm^2/s and 0.74 μm/s, respectively, consistent with the stage 3 movement. Additionally, the viruses moving in nocodazole-treated MDCK cells (nocodazole is a drug to disrupt the microtubules) showed that the virus was moving slowly around the cytomembrane in the nocodazole-treated cell (Figure 4c,d), indicating the movement of the virus was limited around the cytomembrane and the fast and unidirected movement was related to microtubules. The duration of the rapid and directed microtubule-based movements was just a few seconds (Figure S4 in Supporting Information), consistent with the previous report.[3] The results indicated that the stage 3 movement was microtubule-dependent.

The intermittent movement in the perinuclear region was stage 4. On the basis of the dependence of MSD on time, the stage 4 movement was also directed with D and V values of 0.01 μm^2/s and 0.21 μm/s, respectively (Figure 4h). However, why the virus moved intermittently in this stage and whether the movement was related with microtubules remained to be answered.

Likewise, the viruses moved confinedly in the perinuclear region in stage 5. The MSD−time plot showed

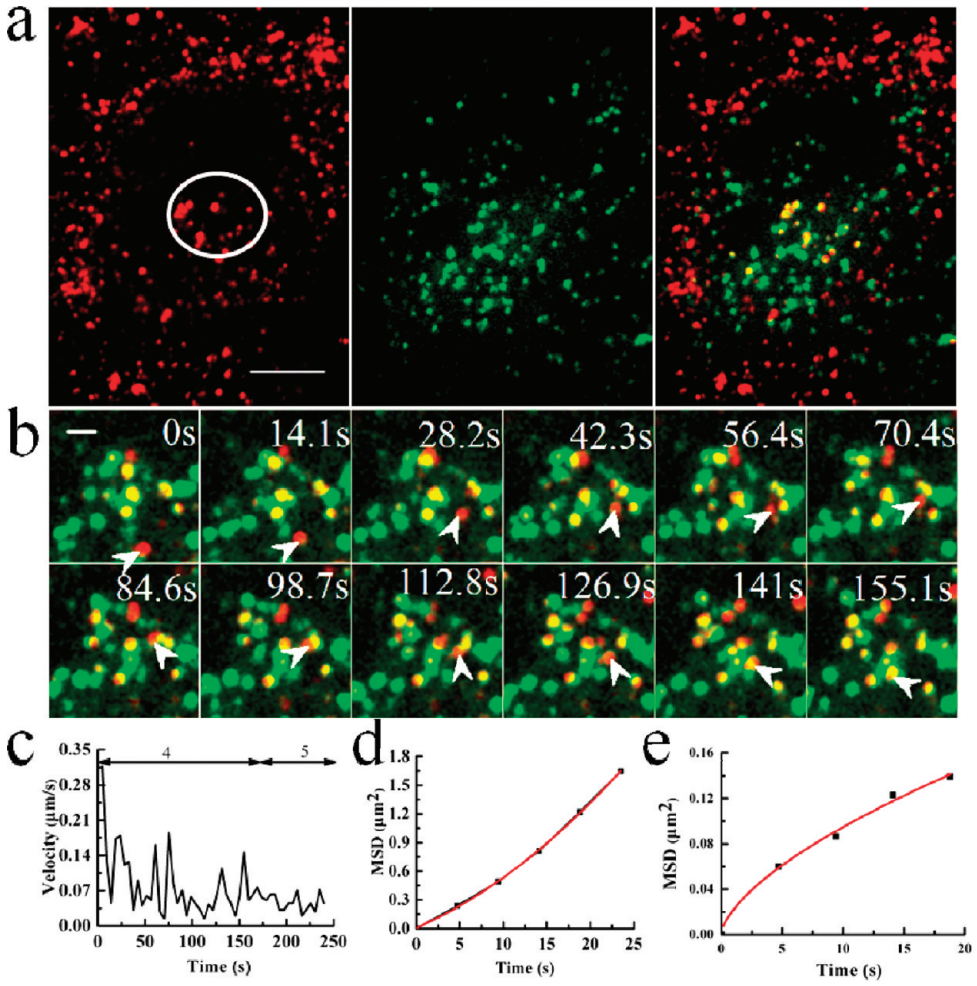

Figure 6. Viruses being transported to acidic endosomes around the MTOC. (a) Fluorescence images of the cell incubated with QD-labeled viruses (red), the acidic endosomes (green), and the merge (scale bar, 10 μm). The white circle indicates the MTOC. (b) Snapshots of a virus (red) converging to an acidic endosome (green) (scale bar, 2 μm). (c) Time trajectory of the virus instantaneous speed shown in (b). Numbers 4 and 5 indicate the duration in stage 4 and stage 5. (d,e) MSD−time plots (black symbols) in stage 4 and stage 5. The red line is a fit to MSD = $4D\tau + (V\tau)^2$ + constant in (d). The red line is a fit to MSD = $4D\tau^{\alpha}$ + constant in (e).

that the movement was in anomalous diffusion mode with D and α values of 0.003 $\mu m^2/s$ and 0.5, respectively, suggesting that the virus may be confined in some cell organelles (Figure 4e). The role of the organelles for virus infection needed to be investigated.

Dynamics of Virus Transports in the Perinuclear Region. Real-time tracking of the viruses in MDCK cells expressing GFP-tagged microtubules (Figure 5a) revealed that the viruses were spatially colocalized with microtubules in the perinuclear region, indicating that viruses converged toward the MTOC, the site of microtubule nucleation.[31] Meanwhile, when the virus movements around the MTOC was monitored (Figure 5b and movie S5 in Supporting Information), it was evident to find that the viruses were moving slowly. The downward-curving MSD−time plots of four virus trajectories showed that the viruses were in anomalous diffusion mode, suggesting that the viruses were confined into some organelles around the MTOC (Figure 5c). The result indicated that the stage 4 movements were also microtubule-dependent, and the viruses were confined in some organelles finally (stage 5).

It was reported that influenza viruses were fused with acidic endosomes for genome release.[3,18] To verify whether the organelles mentioned above were acidic endosomes around the MTOC, the viruses and acidic vesicles were tracked simultaneously in real time in MDCK cells stained with Lysotracker green, a late endolysosomal compartment dye to label acidic compartments.[37] The QD signals were spatially colocalized with the Lysotracker green signals around the MTOC, indicating that the viruses indeed anchored to acidic endosomes finally (Figure 6a). Moreover, the dynamical anchoring process of viruses was analyzed, as shown in Figure 6b and movie S6 in Supporting Information, and the virus was moving fast toward an acidic endosome, staying near the vesicle for about 50 s, moving suddenly toward another acidic endosome and finally fusing with the vesicle, demonstrating that

the vesicle−vesicle fusion event implied the viruses entering the same acidic endosomes. The time trajectory of the instantaneous speed of the virus (Figure 6c) suggested a two-stage process: traveling intermittently toward the target acidic vesicle and moving slowly in the vesicle. The MSD−time plots of the two stages showed that the virus was moving intermittently in a directed manner with D and V values of 0.01 $\mu m^2/s$ and 0.03 $\mu m/s$ (Figure 6d), consistent with the stage 4 movement, followed by moving confinedly in the acidic endosome in anomalous diffusion mode with D and α values of 0.005 $\mu m^2/s$ and 0.6, consistent with the stage 5 movement (Figure 6e). The results indicated that the viruses were interacting with the acidic vesicle in stage 4 movement and finally were confined in the target acidic endosome in stage 5 movement.[3]

To test the relationship between the vesicle−vesicle fusion and the virus−endosome fusion around the MTOC, we infected MDCK cells with dual-labeled viruses (the virus envelope and genome were labeled by 540 nm QDs and Syto 82, respectively) and imaged the viruses at different postinfection in live cells (Figure S5 in Supporting Information). It was found the dual-labeled viruses were on the cell surface at 0 min postinfection. The larger vesicles containing QDs and Syto 82 signals appeared in the perinuclear region within 30 min postinfection, indicating that the viruses were accumulated at the MTOC and the vesicle−vesicle fusion event occurred before genome release. Additionally, the infection pathway of influenza was examined by TEM. The virus infection was displayed by ultrastructural analysis as follows: viruses on the cell surface were trapped into vesicles and transported in the cytoplasm, vesicles containing viruses fused together, and finally viruses fused with large vesicles (Figure S6 in Supporting Information). It was speculated that the virus−endosome fusion event occurred in the late endosomes for genome release around the MTOC, just as the previous reports.[3,7,18]

The above results indicated that the entire virus infection was a five-stage process transport pattern: viruses staying confinedly on the cell surface (stage 1), moving slowly on actin filaments in the cell periphery (stage 2), traveling rapidly on microtubules to the MTOC (stage 3), moving intermittently on microtubules for interacting with acidic endosomes around the MTOC (stage 4), and moving confinedly in acidic endosomes for genome release (stage 5).

In conclusion, the goal of this study was to develop a systemic technique to effectively and efficiently monitor the virus infection behaviors. QD-based single-particle tracking technique was realized for globally visualizing the virus infection behaviors in individual cells in real time and long term, which allowed us to obtain mechanistic and dynamic insights into the population infection behaviors of influenza virus in live cells and to address directly how influenza viruses exploit the endocytosis for infection.

It was reported previously that the movement of influenza viruses was a striking three-stage active transport pattern.[3] In contrast, our data suggest that the virus infection was a five-stage process. After reaching the MTOC *via* microtubules, the viruses move between the acidic endosomes and finally enter the target endosome, which may be a vivid portrayal of the acidification process.

MTOC is the aggregation site of the misfolded proteins, where they would be refolded with the help of chaperones or degraded by the proteasome.[38,39] Viruses may be treated as the misfolded proteins at MTOC for degradation by proteasomes,[2,38,40] which was termed "MTOC rescue" model. This work may be a better description about the MTOC rescue model for virus infection.[2] It was found that the viruses were aggregated to the acidic endosomes around the MTOC followed by a virus−endosome fusion event, which implied that the MTOC may be the replication site of influenza virus.[2,41,42]

QD-based single-particle tracking has been used for studying the virus infection recently.[31−33] Herein, studying the population infection behaviors in real time and long term has been first realized. The present study has enriched the knowledge on cytoplasmic transports and revealed previously unreported aspects on infection mechanisms. The mechanistic and dynamic insights into the virus infection provide a further understanding on virus pathogenesis. This report may offer a reasonable thinking about antiviral drug design. The QD-based single-particle tracking technique would be a powerful and indispensable tool to investigate virus infection mechanisms and to explore the secrets of cytoplasmic transport in the future.

MATERIALS AND METHODS

Virus and Cell. Avian influenza A virus (H9N2) strain was produced in the allantoic cavity of 10 day old embryonated eggs for 48 h at 37 °C. Subsequently, the virions were concentrated by ultracentrifugation for 90 min at 110 000*g* and further purified on sucrose density gradients (15−60%, wt/vol) by ultracentrifugation for 90 min at 110 000*g*. The section between 15 and 37.5% sucrose density was harvested, aliquoted, and stored at −70 °C. The virus was quantitated by protein quantification method. MDCK cells were maintained in culture medium (Dulbecco's modified Eagle medium (DMEM, Gibco) with 10% fetal bovine serum (FBS, Gibco), 100 U/mL penicillin G, and 100 $\mu g/mL$ streptomycin sulfate) at 37 °C in a 5% CO_2 incubater and passaged every 2−3 days. For fluorescence imaging, MDCK cells were seeded onto a 35 mm glass-bottomed Petri dish (NEST Corp) and cultured for 24 h.

Preparation of the Labeled Virus. To realize viruses labeled with QDs, first the viruses were modified with biotin. The viruses were incubated with EZ-Link Sulfo-NHS-LC-Biotin (Thermo) for 2 h at room temperature. Unbound biotinylating agent was removed by gel filtration on a NAP-5 column (GE Healthcare). Virus aggregates were removed with 0.22 μm pore size filters before fluorescence imaging. Subsequently, the biotinylated viruses were labeled with SA-QDs (Wuhan Jiayuan Quantum Dots Co., Ltd., China) using previously published two-step methods.[30] Briefly, the viruses (0.1 mg/mL) were added to the MDCK cells and then labeled with SA-QDs (1 nM) on the cell surface *via* biotin−streptavidin interaction. To obtain dual-labeled viruses, the viruses were incubated with 50 μM Syto 82 at 37 °C for 4 h, biotinylated, and then labeled with QDs as mentioned above.

Virus Infectivity. MDCK cells were cultured in 35 mm Petri dishes for 24 h. When the cells reached 80−90% confluency, they were washed twice with Tyrode plus buffer (135 mM NaCl, 10 mM KCl, 0.4 mM $MgCl_2$, 1 mM $CaCl_2$, 10 mM HEPES, 5.6 mM glucose, and 0.1% BSA, pH 7.4), incubated with H9N2, biotin−H9N2, and biotin−H9N2 at the same concentration at 4 °C for 10 min and washed with Tyrode plus buffer three times. One of the Petri dishes with biotin−H9N2 was added with SA-QDs, maintained at 4 °C for 10 min, and washed three times. Then the infected cells were cultured in infection culture media (DMEM containing 20 μg/mL trypsin, 0.2% BSA, 100 U/mL penicillin G, and 100 μg/mL streptomycin sulfate) for 48 h. The culture medium supernatants of the cells were taken and stored at −70 °C until titer determinations. Titers of the aliquots were determined in triplicate by TCID 50 assay and immunofluorescence focus assay.

In the TCID 50 assay, MDCK cells were cultured in 96-well plates in culture medium until the cells reached 80−90% confluency. The culture medium supernatants were $10^{0.5}$-fold diluted ranging from $10^{-0.5}$ to 10^{-6} in infection media. The MDCK cells were washed twice with PBS and incubated with 100 μL of the diluted virus sample at 37 °C for 1 h. Then the medium was removed and 100 μL of fresh infection medium was added. The infected cells were cultured at 37 °C for 72 h. The cytopathic effect was observed daily and confirmed by hemagglutination assay. Twenty-five microliters of culture supernatants was put in V-bottom plates, and 25 μL of 1% chicken red blood cells was added in each well. The plates were maintained at 37 °C for 45 min, and the hemagglutination patterns were examined by eye. The titer was calculated based on the Reed and Muench method.

In the immunofluorescence focus assay, the culture medium supernatants were $10^{0.5}$-fold diluted ranging from 10^{-1} to $10^{-2.5}$, added onto the MDCK cell monolayers for 1 h at 37 °C, and then removed. The cells were maintained in DMEM at 37 °C for 48 h, washed three times, fixed with 4% paraformaldehyde, followed by immunofluorescence staining. For each sample, 20 random microscopic fields were examined for immunofluorescent focus counting. The number of immunofluorescent focus units (IFU) of virus was obtained as follows: titer = (the average number of the IFU per field) × (the number of fields per well) × (the dilution of the virus)$^{-1}$.

Transfection of Cells. The MDCK cells were transiently transfected with the plasmids of GFP-mouse talin to label actin filaments and GFP−microtubule-associated protein 4 to label microtubules[43,44] using lipofectamine LTX transfection reagent (Invitrogen). For a 20 mm Petri dish to be transfected, 1 μL of lipofectamine LTX reagent was combined with Opti-MEM I reduced serum medium (Gibco) and 0.5 μg of DNA for a final volume of 100 μL. Lipofectamine LTX-DNA mixture was incubated at room temperature for 30 min, added to the cell culture, and then incubated in a 5% CO_2 environment. Medium was changed after 6 h.

Immunofluorescence. Cells incubated with viruses were fixed in 4% (w/v) paraformaldehyde for 20 min. After washing with PBS, cells were exposed in PBS containing 5% (w/v) BSA for 30 min. Then the cells were incubated with the monoclonal antibody against HA at 37 °C for 1.5 h. The cells were then washed extensively with PBS containing 1% BSA and incubated with Dylight 649-conjugated goat anti-mouse IgG (Thermo) at 37 °C for 45 min.

Fluorescence Imaging. A spinning-disk confocal microscope (Andor Revolution XD) was equipped with an Olympus IX 81 microscope, a Nipkow disk type confocal unit (CSU 22, Yokogawa), a CO_2 online culture system (INUBG2-PI), and an EMCCD (Andor iXon DV885K single photon detector). Excitation and emission filters were as follows: 605 nm QDs/Syto 82, 561 nm excitation, emission BP 617/73 nm; 540 nm QDs/GFP/Lysotracker green/DiO, 488 nm excitation, emission BP 525/50 nm filters; Dylight 649, 640 nm excitation, emission BP 685/40 nm filter. For simultaneous two-color imaging, the fluorescence was imaged alternately onto the EMCCD by two channels.

Imaging Analysis. Each frame in the movies was processed by a gauss filter to remove background noise. To track and analyze the movements of the particles, the trajectories were generated by pairing spots in each frame according to proximity and similarity in intensity. Only those particles that moved roughly within the focal plane were used for single-particle tracking analysis. Colocalizations of viruses with cellular markers were indentified with Imaging-Pro-Plus software and confirmed by eye. The criteria for colocalization were that the objects were together and had at least partial overlap. MSD was calculated by the user-written program with Matlab software.[36] The criteria for extracting the perinuclear region are where the viruses were accumulated and at the same time the rapid and unidirected virus movements disappeared.

Acknowledgment. We thank Zhi-Gang Wang and Li-Juan Zhang for their suggestions. This work was supported by the National Basic Research Program of China (973 Program, Nos. 2011CB933600 and 2006CB933100), the Science Fund for Creative Research Groups of NSFC (Nos. 20921062 and 20621502), the National Natural Science Foundation of China (20833006 and 21005056), and the "3551 Talent Program" of the Administrative Committee of East Lake Hi-Tech Development Zone ([2011]137).

Supporting Information Available: Figures S1−S6 and movies S1−S6. This material is available free of charge *via* the Internet at http://pubs.acs.org.

REFERENCES AND NOTES

1. Greber, U. F.; Way, M. A Superhighway to Virus Infection. *Cell* **2006**, *124*, 741–754.
2. Leopold, P. L.; Pfister, K. K. Viral Strategies for Intracellular Trafficking: Motors and Microtubules. *Traffic* **2006**, *7*, 516–523.
3. Lakadamyali, M.; Rust, M. J.; Babcock, H. P.; Zhuang, X. W. Visualizing Infection of Individual Influenza Viruses. *Proc. Natl. Acad. Sci. U.S.A.* **2003**, *100*, 9280–9285.
4. van der Schaar, H. M.; Rust, M. J.; Waarts, B. L.; van der Ende-Metselaar, H.; Kuhn, R. J.; Wilschut, J.; Zhuang, X.; Smit, J. M. Characterization of the Early Events in Dengue Virus Cell Entry by Biochemical Assays and Single-Virus Tracking. *J. Virol.* **2007**, *81*, 12019–12028.
5. Brandenburg, B.; Zhuang, X. Virus Trafficking—Learning from Single-Virus Tracking. *Nature* **2007**, *5*, 197–208.
6. Marsh, M.; Helenius, A. Virus Entry: Open Sesame. *Cell* **2006**, *124*, 729–740.
7. Mercer, J.; Schelhaas, M.; Helenius, A. Virus Entry by Endocytosis. *Annu. Rev. Biochem.* **2010**, *79*, 803–833.
8. Vaughan, J. C.; Brandenburg, B.; Hogle, J. M.; Zhuang, X. Rapid Actin-Dependent Viral Motility in Live Cells. *Biophys. J.* **2009**, *97*, 1647–1656.
9. van der Schaar, H. M.; Rust, M. J.; Chen, C.; van der Ende-Metselaar, H.; Wilschut, J.; Zhuang, X.; Smit, J. M. Dissecting the Cell Entry Pathway of Dengue Virus by Single-Particle Tracking in Living Cells. *PLoS Pathog.* **2008**, *4*, e1000244.
10. Chen, C.; Zhuang, X. W. Epsin 1 Is a Cargo-Specific Adaptor for the Clathrin-Mediated Endocytosis of the Influenza Virus. *Proc. Natl. Acad. Sci. U.S.A.* **2008**, *105*, 11790–11795.
11. Thomas, J. K.; Noppenberger, J. Avian Influenza: A Review. *Am. J. Health-Syst. Pharm.* **2007**, *64*, 149–165.
12. Skeik, N.; Jabr, F. Influenza Viruses and the Evolution of Avian Influenza Virus H5N1. *Int. J. Infect. Dis.* **2008**, *12*, 233–238.

13. Lee, C. W.; Saif, Y. M. Avian Influenza Virus. *Comp. Immunol. Microbiol. Infect. Dis.* **2009**, *32*, 301–310.
14. Wong, S. S.; Yuen, K. Y. Avian Influenza Virus Infections in Humans. *Chest* **2006**, *129*, 156–168.
15. Capua, I.; Alexander, D. Avian Influenza and Human Health. *Acta Trop.* **2002**, *83*, 1–6.
16. Peiris, J. S. M.; de Jong, M. D.; Guan, Y. Avian Influenza Virus (H5N1): A Threat to Human Health. *Clin. Microbiol. Rev.* **2007**, *20*, 243–267.
17. Neumann, G.; Chen, H.; Gao, G. F.; Shu, Y.; Kawaoka, Y. H5N1 Influenza Viruses: Outbreaks and Biological Properties. *Cell Res.* **2009**, *20*, 51–61.
18. Lakadamyali, M.; Rust, M. J.; Zhuang, X. Endocytosis of Influenza Viruses. *Microbes Infect.* **2004**, *6*, 929–936.
19. Sieczkarski, S. B.; Whittaker, G. R. Dissecting Virus Entry *via* Endocytosis. *J. Gen. Virol.* **2002**, *83*, 1535–1545.
20. Rust, M. J.; Lakadamyali, M.; Zhang, F.; Zhuang, X. Assembly of Endocytic Machinery around Individual Influenza Viruses during Viral Entry. *Nat. Struct. Mol. Biol.* **2004**, *11*, 567–573.
21. Xing, Y.; Xia, Z.; Rao, J. Semiconductor Quantum Dots for Biosensing and *In Vivo* Imaging. *IEEE Trans. Nanobiosci.* **2009**, *8*, 4–12.
22. Ciarlo, M.; Russo, P.; Cesario, A.; Ramella, S.; Baio, G.; Neumaier, C. E.; Paleari, L. Use of the Semiconductor Nanotechnologies "Quantum Dots" for *In Vivo* Cancer Imaging. *Recent Pat. Anti-Cancer Drug Discovery* **2009**, *4*, 207–215.
23. Michalet, X.; Pinaud, F. F.; Bentolila, L. A.; Tsay, J. M.; Doose, S.; Li, J. J.; Sundaresan, G.; Wu, A. M.; Gambhir, S. S.; Weiss, S. Quantum Dots for Live Cells, *In Vivo* Imaging, and Diagnostics. *Science* **2005**, *307*, 538–544.
24. Medintz, I. L.; Uyeda, H. T.; Goldman, E. R.; Mattoussi, H. Quantum Dot Bioconjugates for Imaging, Labelling and Sensing. *Nat. Mater.* **2005**, *4*, 435–446.
25. Gao, X. H.; Yang, L. L.; Petros, J. A.; Marshal, F. F.; Simons, J. W.; Nie, S. M. *In Vivo* Molecular and Cellular Imaging with Quantum Dots. *Curr. Opin. Biotechnol.* **2005**, *16*, 63–72.
26. Bentolila, L. A.; Ebenstein, Y.; Weiss, S. Quantum Dots for *In Vivo* Small-Animal Imaging. *J. Nucl. Med.* **2009**, *50*, 493–496.
27. Li, F.; Zhang, Z. P.; Peng, J.; Cui, Z. Q.; Pang, D. W.; Li, K.; Wei, H. P.; Zhou, Y. F.; Wen, J. K.; Zhang, X. E. Imaging Viral Behavior in Mammalian Cells with Self-Assembled Capsid-Quantum-Dot Hybrid Particles. *Small* **2009**, *5*, 718–726.
28. Chang, Y. P.; Pinaud, F.; Antelman, J.; Weiss, S. Tracking Bio-Molecules in Live Cells Using Quantum Dots. *J. Biophotonics* **2008**, *1*, 287–298.
29. Lidke, D. S.; Nagy, P.; Heintzmann, R.; Arndt-Jovin, D. J.; Post, J. N.; Grecco, H. E.; Jares-Erijman, E. A.; Jovin, T. M. Quantum Dot Ligands Provide New Insights into ErbB/HER Receptor-Mediated Signal Transduction. *Nat. Biotechnol.* **2004**, *22*, 198–203.
30. Liu, S. L.; Zhang, Z. L.; Sun, E. Z.; Peng, J.; Xie, M.; Tian, Z. Q.; Lin, Y.; Pang, D. W. Visualizing the Endocytic and Exocytic Processes of Wheat Germ Agglutinin by Quantum Dot-Based Single-Particle Tracking. *Biomaterials* **2011**, *32*, 7616–7624.
31. Luo, K.; Li, S.; Xie, M.; Wu, D.; Wang, W. X.; Chen, R.; Huang, L. Q.; Huang, T.; Pang, D. W.; Xiao, G. F. Real-Time Visualization of Prion Transport in Single Live Cells Using Quantum Dots. *Biochem. Biophys. Res. Commun.* **2010**, *394*, 493–497.
32. Liu, H.; Liu, Y.; Liu, S.; Pang, D. W.; Xiao, G. Clathrin-Mediated Endocytosis in Living Host Cells Visualized through Quantum Dot Labeling of Infectious Hematopoietic Necrosis Virus. *J. Virol.* **2011**, *85*, 6252–6262.
33. Joo, K. I.; Fang, Y.; Liu, Y.; Xiao, L.; Gu, Z.; Tai, A.; Lee, C. L.; Tang, Y.; Wang, P. Enhanced Real-Time Monitoring of Adeno-Associated Virus Trafficking by Virus-Quantum Dot Conjugates. *ACS Nano* **2011**, *5*, 3523–3535.
34. Cross, K. J.; Burleigh, L. M.; Steinhauer, D. A. Mechanisms of Cell Entry by Influenza Virus. *Expert Rev. Mol. Med.* **2001**, *3*, 1–18.
35. Saxton, M. J.; Jacobson, K. Single-Particle Tracking: Applications to Membrane Dynamics. *Annu. Rev. Biophys. Biomol. Struct.* **1997**, *26*, 373–399.
36. Saxton, M. J. Single-Particle Tracking: The Distribution of Diffusion Coefficients. *Biophys. J.* **1997**, *72*, 1744–1753.
37. Sasai, M.; Linehan, M. M.; Iwasaki, A. Bifurcation of Toll-like Receptor 9 Signaling by Adaptor Protein 3. *Science* **2010**, *329*, 1530–1534.
38. Wileman, T. Aggresomes and Pericentriolar Sites of Virus Assembly: Cellular Defense or Viral Design? *Annu. Rev. Microbiol.* **2007**, *61*, 149–167.
39. Kopito, R. R. Aggresomes, Inclusion Bodies and Protein Aggregation. *Trends Cell Biol.* **2000**, *10*, 524–530.
40. Bailey, C. J.; Crystal, R. G.; Leopold, P. L. Association of Adenovirus with the Microtubule Organizing Center. *J. Virol.* **2003**, *77*, 13275–13287.
41. Wileman, T. Aggresomes and Autophagy Generate Sites for Virus Replication. *Science* **2006**, *312*, 875–878.
42. Heath, C. M.; Windsor, M.; Wileman, T. Aggresomes Resemble Sites Specialized for Virus Assembly. *J. Cell Biol.* **2001**, *153*, 449–455.
43. Kost, B.; Spielhofer, P.; Chua, N. H. A GFP-Mouse Talin Fusion Protein Labels Plant Actin Filaments *in Vivo* and Visualizes the Actin Cytoskeleton in Growing Pollen Tubes. *Plant J.* **1998**, *16*, 393–401.
44. Mathur, J.; Chua, N. H. Microtubule Stabilization Leads to Growth Reorientation in Arabidopsis Trichomes. *Plant Cell* **2000**, *12*, 465–477.